

High-Efficiency Lossy Image Coding Through Adaptive Neighborhood Information Aggregation

Ming Lu and Zhan Ma

Abstract—Questing for lossy image coding (LIC) with superior efficiency on both compression performance and computation throughput is challenging. The vital factor behind is how to intelligently explore Adaptive Neighborhood Information Aggregation (ANIA) in transform and entropy coding modules. To this aim, Integrated Convolution and Self-Attention (ICSA) unit is first proposed to form content-adaptive transform to dynamically characterize and embed neighborhood information conditioned on the input. Then a Multistage Context Model (MCM) is developed to stagewise execute context prediction using necessary neighborhood elements for accurate and parallel entropy probability estimation. Both ICSA and MCM are stacked under a Variational Auto-Encoder (VAE) architecture to derive rate-distortion optimized compact representation of input image via end-to-end training. Our method reports the superior compression performance surpassing the VVC Intra with $\approx 15\%$ BD-rate improvement averaged across Kodak, CLIC and Tecnick datasets; and also demonstrates $\approx 10\times$ speedup of image decoding when compared with other notable learned LIC approaches. All materials are made publicly accessible at <https://njuvision.github.io/TinyLIC> for reproducible research.

Index Terms—Lossy Image Compression, Adaptive Neighborhood Information Aggregation, Convolution, Self-Attention, Multistage Context Model

1 INTRODUCTION

THE pursuit of high-efficiency lossy image coding is ever increasingly critical for vast networked applications such as photo sharing, commercial advertisements, remote medical diagnosis, etc. In principle, lossy image coding searches for the *optimal compact representation* of input source in a computationally feasible way that leads to the best rate-distortion (R-D) performance [1] defined in

$$J = R + \lambda D. \quad (1)$$

Here, λ is the Lagrange multiplier that controls the desired compression trade-off between the rate and distortion. R represents the average number of bits needed to encode the input data, and D can be measured in different forms like the Mean Square Error (MSE) and Multiscale Structural Similarity (MS-SSIM).

Though conceptually any input source can be represented using vector quantization, it is practically infeasible for high-dimensional source because of unbearable complexity [2]. In the light of computationally manageable coding solution, it then leads to the *Transform Coding* that divides the image coding problem into three consecutive simple steps, e.g., transform, quantization and entropy coding, as defined in [3].

1.1 Background and Motivation

In general, the “transform” module $G(\cdot)$ ¹ converts a image block in pixel domain to a latent space (e.g., frequency domain), by which less nonzero coefficients are retained to represent the input source [3]; And then “quantization”

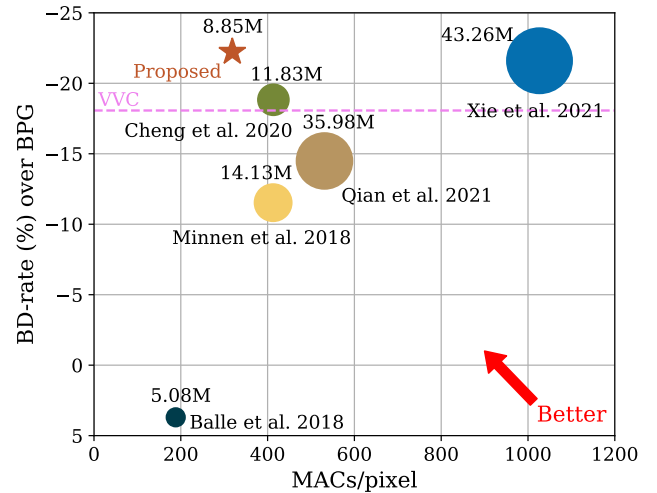


Fig. 1. **Compression Performance versus Complexity.** Performance gain is measured by BD-rate against the HEVC Intra compliant BPG anchor [4] (a.k.a., BPG), and complexity measures include the Multiply-Accumulate Operations per pixel (MACs/pixel) and the size of model parameters. Notable learned LIC methods like Ballé *et al.* 2018 [5], Minnen *et al.* 2018 [6], Xie *et al.* 2021 [7], Qian *et al.* 2021 [8], Cheng *et al.* 2020 [9], as well as the VVC Intra using VTM-12.1, a.k.a., VVC [10] are evaluated for comparison. BD-rate is averaged using all test images in Kodak dataset. RGB images are directly encoded under 444 mode [11], [12]. The proposed method reports the best performance with less MACs/pixel and parameters.

function $Q(\cdot)$ is applied to use finite quantized symbols to represent transformed coefficients with the least bitrate desire under a certain distortion target [13]. To ensure the least bitrate consumption, “entropy coding” engine $E(\cdot)$ is

M. Lu and Z. Ma are with the Nanjing University, Nanjing, Jiangsu 210093, China. Email: luming@mail.nju.edu.cn, mazhan@nju.edu.cn.

1. Usually a transform module is comprised of a pair of analysis $g_a(\cdot)$ (or forward) and synthesis $g_s(\cdot)$ (or backward) functions.

typically devised to further reduce statistical redundancy by accurately and efficiently modeling the probability distribution of each quantized symbol [14]. Usually, finetuning the transform, quantization and entropy coding jointly is enforced for past decades to pursue better image compression [10], [15]–[17].

Since uniform or scalar quantizer is extensively applied in mainstream image compression solutions, we keep the use of it and have the main focus of this work on the development of transform and entropy coding.

- 1) **Transform Function.** Since the 1970s, a great amount of studies have been devoted to advance the transform module, from the very first Discrete Cosine Transform (DCT) [18], to variable-size Karhunen-Loève Transform (KLT) [19], to Hybrid intra Prediction/Transform (HiPT) that applies spatial intra prediction and residue DCT across variable-size tree blocks [11], [12], [15], and to Convolutional Neural Network (CNN) based nonlinear Transform [2] with the support of attention mechanism [9], [20]. All of these endeavors give a clear direction: exploiting redundancy exhaustively with better energy compaction desires content-adaptive transforms that can *dynamically characterize the neighborhood distribution* across a variety of scales according to the input.
- 2) **Entropy Probability Model.** As revealed in a serial image/video coding standards, context-adaptive arithmetic coding demonstrates its superior capacity to model non-stationary and high-order statistics among syntax elements (e.g., quantized coefficients). Unlike transforms that can use block-level parallelism to some extent [21], entropy model, especially in decoding phase, operates sequentially because of causal dependency [14]. Thus, high-performance and high-throughput entropy modeling is of great importance in practice [22]. How to *leverage neighborhood dependency* to not only provide accurate probability estimation, but also assure computationally-efficient processing of underlying context model in entropy coding is crucial.

As seen, the vital factor behind high-efficiency LIC for ensuring high-performance compression and high-throughput computation jointly is highly related to the efficient use of neighborhood information that is defined as the *Adaptive Neighborhood Information Aggregation* (ANIA).

1.2 Our Method

This work therefore devises solutions to fulfill the use of ANIA in respective transform and entropy coding modules for high-efficiency LIC.

Content-Adaptive Transform Through Integrated Convolution & Self-Attention. Past explorations have suggested us to leverage neighborhood dependency adaptively for better transformation [12], [19]. Although deep CNN based nonlinear transforms have been devised in a collection of learned LIC approaches shown in Fig. 1 because of their powerful representation capacity to embed neighborhood information of underlying content, they do have

TABLE 1
Notations

Abbr.	Description
ANIA	Adaptive Neighborhood Information Aggregation
ICSA	Integrated Convolution and Self-Attention
RSTB	Residual Swin Transformer Block
MCM	Multistage Context Model
VAE	Variational Auto-Encoder
LIC	Lossy Image Coding
MAC	Multiply-Accumulate Operation
BD-rate [28]	Bjontegaard Delta Rate
PSNR	Peak Signal-to-Noise Ratio
MSE	Mean Square Error
MS-SSIM [29]	Multiscale Structural Similarity
BPG	Better Portable Graphics
HEVC [4]	High-Efficiency Video Coding
VVC [10]	Versatile Video Coding

notable limitation [23], e.g., offline trained or pretrained CNN models are presented with fixed weights for the use in inference, making them generally inefficient for unseen images that exhibit different content distribution from training samples [24].

To tackle it, we propose the Integrated Convolution and Self-Attention (ICSA) unit that is comprised of a convolutional layer and multiple self-attention layers realized by Residual Swin Transformer Blocks (RSTBs) [25] to adaptively aggregate neighborhood information (elements) through attention based weighting conditioned on the input. In comparison to fixed-weights convolutions used in pretrained CNN models, self-attention mechanism in RSTB can weigh and aggregate elements across neighboring windows on-the-fly with which instantaneous content dynamics can be better captured to some extent. Note that we often apply spatial resampling at convolutional layer in each ICSA unit to not only reduce the data dimensionality [20] but also exploit the hierarchical characteristics of the content [19].

Entropy Coding Using Multistage Context Model. Adaptive context modeling conditioned on joint hyperprior and autoregressive neighbors that was originally proposed by Minnen *et al.* [6] and extended in succeeding followups [9], [20], [26] has shown remarkable capacity to accurately approximate the entropy probability of latent features. For simplicity, we call it autoregressive (AR) model in short. However, the sequential processing of autoregressive neighbors makes the image decoder extremely impractical, e.g., taking hours to reconstruct a 1080p RGB image due to element-by-element computation as reported in [20], [27]².

Thus, having a method that not only best maintains the performance of AR model but also enables parallel processing for high-throughput computation is of great desire. Apparently, the efficiency of AR model comes from the exploration of causal neighbors in a raster scan order spatially (see spatially-ordered elements in Fig. 5a as an example). Simply enforcing the independent processing of each element and completely ignoring the inter-element depen-

² Image encoding speedup can be easily fulfilled by parallel processing since elements are all available but the casual dependency in image decoding enforces the sequential processing strictly.

dency for massive concurrency can improve the throughput but definitely deteriorates the compression performance. It urgently calls for an alternative spatial patterning to intelligently exploit neighborhood correlation using a different scan order.

He *et al.* [30] firstly introduces the checkerboard pattern for spatial arrangement of neighborhood context modeling. By re-organizing the decoding order, it achieves significantly improved computational efficiency. However, half of the latents in their method are predicted only depend on the hyperpriors and the contextual information will not be fully utilized, which may constraint the performance to some extent.

Motivated by this, we propose the Multistage Context Model (MCM) to stagewise estimate the entropy probability in parallel. To this aim, we spatially group elements into non-overlapped 2×2 element blocks in latent feature map³. The same element numbering in an order of upper-left ("0"), bottom-right ("1"), upper-right ("2"), and bottom-left ("3") is applied for all 2×2 blocks. Elements marked with the same number are processed concurrently, and context prediction is enforced following the order of element numbering (see Fig. 5c). In this way, neighborhood correlation is adaptively exploited from one stage to another (see Fig. 6a). As seen, the proposed MCM not only retains the high efficiency due to the use of valid and abundant neighbors in 3×3 local window (not just causal neighbors) for probability estimation, but also offers the high-throughput computation by fully paralleling all elements at each stage.

End-to-End Architecture. We later stack aforementioned ICSA and MCM units upon the prominent VAE structure with a scale hyperprior shown in Fig. 2 to form the a novel learned LIC. For short, we call it *TinyLIC*. Such VAE architecture has been well generalized in various learned LIC solutions [5], [6], [9], [20]. As seen, main and hyper coders are paired with encoding and decoding processes. In main encoder, it generally performs the analysis transform $g_a(\cdot)$ using four consecutive ICSA units to derive latent features of input image x while the main decoder mirrors the encoding as the synthesis transform $g_s(\cdot)$ to reconstruct input image \hat{x} . To efficiently encode quantized latent features, MCM is used to jointly use hyperpriors and available local neighbors for accurate and high-throughput entropy probability estimation, where hyperpriors are generated by the hyper coder that shares the same paired structure as the main coder while just using two ICSA units and simple factorized entropy model [5], [6].

1.3 Contribution

Our contributions are summarized as below:

1) This work shows that high-efficiency LIC with both high-performance compression and high-throughput computation can be successfully fulfilled by adaptive neighborhood information aggregation (ANIA) to best exploit neighborhood characteristics in transform and entropy coding; As for transform function, the proposed ANIA dynamically

adapts itself to the input to best characterize and embed neighborhood information; while for entropy coding, the proposed ANIA enables adaptive context modeling through an alternative neighborhood scanning order to not only retain the efficiency as the AR model but also enables high-throughput parallel processing.

2) This work exemplifies the design of ANIA by using the Integrated Convolution and Self-Attention unit as content-adaptive transform, and by applying the Multistage Context Model in entropy coding, respectively, to form the proposed *TinyLIC*; Extensive comparisons report the the superior compression performance of *TinyLIC*, e.g., averaged $\approx 15\%$ BD-rate gain against the VVC Intra for three popular datasets, and simultaneously offer almost $10\times$ speedup of image decoding to notable learned LIC approaches.

3) The proposed *TinyLIC* further reports its robustness by comprehensively examining a variety of settings in modular components such as the backbone structure (e.g., token embedding method, attention window size, large-kernel convolution versus ICSA), entropy context model (e.g., alternative schemes, context modeling insights) in ablation studies. Additional experiments are also carried out to report the generalization of the *TinyLIC* for the support of different input sources, variable-rate adaptation with limited models, in-loop quality enhancement, etc in a companion supplementary material at our website.

2 RELATED WORK

This section briefs the developments in transform coding for image compression including classical rules-based approaches and recently-emerged learning-based solutions.

2.1 Rules-based Transform Coding

2.1.1 Transform Function

Fixed-Weights Transforms. Prominent transform modules like Discrete Cosine Transform (DCT) [18] and Wavelet Transform [31] use linear transformations that are generally comprised of a set of linear and orthogonal basis functions. They have been used in famous image coding standards like JPEG [32] and JPEG2000 [33]. Later, DCT alike Integer transform functions [34] are adopted in intra profile of respective H.264/AVC [35], HEVC [4], and VVC [10] to process predictive residues.

Apparently, linear transformation with fixed basis can not best exploit the redundancy because the content of underlying image block is non-stationary and does not strictly follow the mathematical distribution as assumed (e.g., Gaussian source [3]). Therefore, devising transformation with data-driven basis to better exploit non-stationary content distribution attracts intensive attention. Notable approaches include the dictionary learning [36]–[38], KLT [19] and recently-emerged CNN transforms [2] (see Sec. 2.2 for more details). Note that transforms with data-driven basis are also with fixed weights after training.

Content-Adaptive Transforms. Although data-driven transforms have improved energy compaction [19] to some extent compared with fixed-basis DCT or wavelet, the model generalization is still a challenging problem due to

3. In fact, a 2×2 element block is a vectorized tensor at a size of $2 \times 2 \times c$ with c channels. Since we perform the context modeling in spatial domain for all channels at one time, we typically omit the channel dimension in discussion for simplicity.

fixed weights after training. For example, if the distribution of test data is different from the training samples, energy compaction is largely suffered with poor coding performance [19].

Given that neighborhood pixels often present high coherency, adaptively weighting local spatial neighbors through an autoregressive predictive means [39] or pre-defined directional patterns [11], [12] had been proposed and extensively studied over decades. Since the late 1990s, spatial intra prediction was integrated with aforementioned fixed-basis transforms (e.g., DCT), forming the normative toolset in mainstream intra profiles of video coding standards like H.264/AVC Intra, HEVC Intra, and VVC Intra, because of the superior performance on redundancy removal and energy compaction [19].

Such Hybrid intra Prediction/Transform (HiPT) dynamically characterizes and embeds spatial neighbors, making it content adaptive. Then after, variable-size HiPT has been extended along with the recursive tree structures, by which the non-stationary image characteristics in different regions can be well and adaptively captured and modeled.

The use of reconstructed neighbors in HiPT leverages the neighborhood coherency through handcrafted rules to best reflect the dynamics of the input content, which motivates us to develop the content-adaptive transform from a learning perspective.

2.1.2 Entropy Model

Quantized transform coefficients are subsequently encoded into binary strings for efficient storage or network delivery, by further exploiting their statistical correlation. Extensive explorations conducted in the past [14] have clearly revealed that an accurate context model conditioned on neighborhood elements plays the vital role for high-efficiency entropy coding. Examples include the context-adaptive variable-length coding (CAVLC) and context-adaptive binary arithmetic coding (CABAC) [14]. And, because of the superior efficiency offered by the arithmetic codes, adaptive arithmetic coding, e.g., CABAC and its variants, is widely deployed in mainstream compression recommendations like HEVC, VVC, JPEG2000, etc, where associated context models are mainly developed following empirical rules and experimental observations.

Computation throughput limitation incurred by the sequential data dependency in entropy context modeling was extensively investigated since the standardization of HEVC a decade ago. High-throughput and high-performance were then jointly evaluated during the development of entropy coding engine [22], [40]. Well-known examples include symbol parsing dependency unknitting, bins grouping, etc that more or less rely on the utilization of contextual correlation in local neighborhood.

2.2 Learning-based Transform Coding

2.2.1 End-to-End Learned LIC

Given that learned LIC methods jointly optimize transform and entropy coding modules through end-to-end learning, we review them together.

CNN Models. As CNNs have shown their remarkable capacity on characterizing and embedding compact representation features from underlying image data for various visual tasks, numerous attempts have been made in recent years to use CNN models for image compression. For instance, back to 2017, Ballé *et al.* [41] showed that stacked convolutional layers could replace the traditional transforms to form an end-to-end trainable image compression method with better efficiency than the JPEG [16], in which a CABAC alike entropy coding engine was used. Then after, hyper priors and autoregressive neighbors were introduced and jointly used in [6], [9], [20] under the VAE architecture for entropy context modeling assuming the Gaussian distribution, further improving the image compression efficiency. As seen such a context model conditioned joint hyperprior and autoregressive neighbors mostly utilized the local correlations in published works. Recently, Qian *et al.* [8] and Kin *et al.* [42] extended the utilization of local correlation only to joint global and local correlation by the inclusion of additional global reference.

In addition to these methods mainly utilizing convolutions to analyze and aggregate information locally, our early exploration [20] applied a nonlocal attention to optimize intermediate features generated by each convolutional layer for more effective information embedding. However, the nonlocal computation is expensive since it typically requires a large amount of space to host a correlation matrix with size of $HW \times HW$ for a naive implementation. Note that H and W are the height and width for input feature map. Similar convolution-based spatial attention mechanism was also utilized in Cheng *et al.* [9] and other related works.

ViT Models. Learned LIC solutions discussed above mainly leveraged CNNs to formulate nonlinear transform and high-performance entropy coding. As attention mechanism had reported its potentials for better compression efficiency [9], [20], and the surge of the use of self-attention based Vision Transformers (ViT) in various tasks [25], [43]–[47], a number of attempts had been made to apply Transformer alike schemes to improve transform and entropy coding of learned LIC. For example, Zhu *et al.* [48] replaced stacked convolutions with Swin Transformer to form the nonlinear transform and kept using the channel-wise autoregressive contexts as in [49]; while Qian *et al.* [50] retained CNN transform but replaced the convolution-based entropy context engine with the Transformer. Coincidentally at the same time, our preliminary study in [26] extended Transformer architecture to both transform and entropy coding modules.

Discussion. Most works have claimed that the ability of long-range dependency capturing in ViTs improves the near-range dependency exploration in CNN models. Yet, we have a different view: we believe that the compression gains are mainly contributed by the self-attention mechanism that can best weigh neighborhood dynamics of any given content input for information aggregation. As reported in [51] and further confirmed in ablation studies, large-kernel convolutions can also capture relatively long-range dependency as ViTs for various tasks. This is why we formulate the core issue of learned LIC is how to comprehensively explore the ANIA, and the use of either Transformer or CNN or their combination is just a toolset to exemplify the idea.

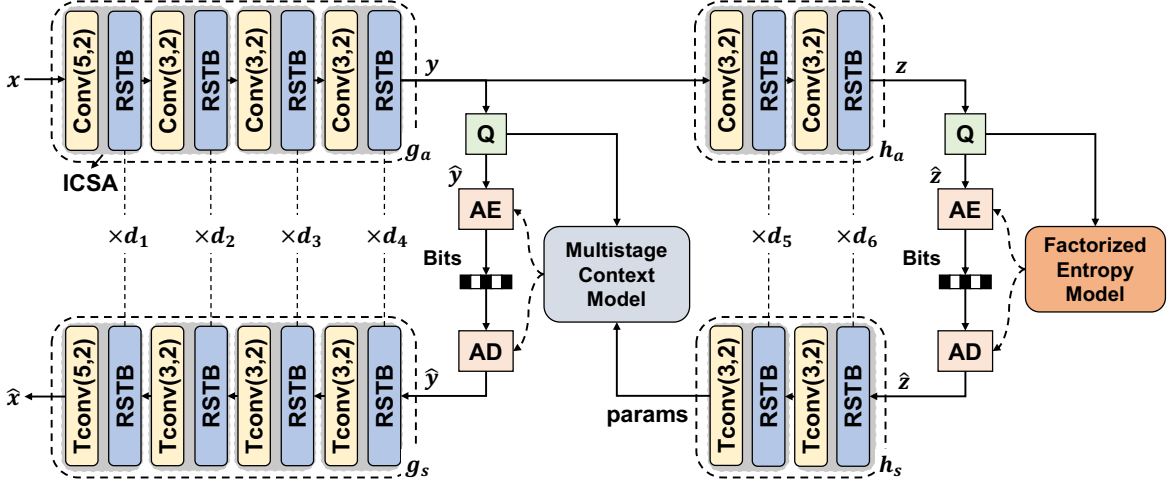


Fig. 2. *TinyLIC*. Prominent VAE structure with a hyperprior is used with main and hyper encoder-decoder pairs. Four and two paired ICSA units are used in main and hyper coders. Each ICSA is comprised of a convolutional layer for token embedding and spatial resampling, and multiple Residual Swin Transformer Blocks (RSTBs) to adaptively aggregate neighborhood information through attention based weighting. $d_i, i = 1, 2, \dots, 6$ is the number of RSTBs used at i -th stage. Convolution $\text{Conv}(k, s)$ and its transpose $\text{Tconv}(k, s)$ apply the kernel at a size of $k \times k$ and a stride of s . $k = 3$ or 5 , and $s = 2$. Multistage Context Model (MCM) is used for latent features by jointly leveraging the hyperpriors and local neighbors and simple factorized entropy model is applied for the coding of hyperpriors. Quantization is used in Q; AE and AD stand for respective Arithmetic Encoding and Decoding.

2.2.2 Efficient Learned LIC

Computation efficiency is another key factor determining whether the solution can be used in practice. Learned LIC approaches were rigorously criticized for the desire of exhaustive resource for computing and caching.

One direction to develop computationally efficient learned LIC is to enable variable-rate support using few pretrained models since most solutions have trained specific model for individual bitrate [52]–[54]. This would reduce the model switching for supporting wider bitrate range, and also decrease the storage requirement for caching multiple models. As shown at our webpage, the proposed *TinyLIC* can be easily extended to support variable-rate compression without noticeable performance loss. In the meantime, to execute learned LIC with less peak memory in inference, native floating-point model could be quantized using integer network [55] and fixed-point network [56].

Another computationally exhaustive subsystem is the context-adaptive entropy coding incurred by sequential processing of syntax elements. For instance, the computational complexity of a native implementation of the popular entropy context model conditioned on joint hyperprior and autoregressive neighbors is a function of $\mathcal{O}(H \times W)$, reporting unbearable time duration for image decoding. Massively-parallel context modeling was then developed by exploring channel-wise concurrency like channel-wise grouping [49], and spatial concurrency like two-stage checkerboard patterning [30] or column-wise/row-wise parallelism [20] to improve the throughput with reasonable performance compromise. The proposed *TinyLIC* explores the multistage context modeling through a 2×2 spatial patterning for context prediction using valid neighbors and stage-wise massive parallelism. Contrast with the checkerboard context modeling in [30], e.g., a typical example of the two-stage spatial patterning shown in Fig. 5b, the proposed MCM provides better compression performance by gradually aggregating

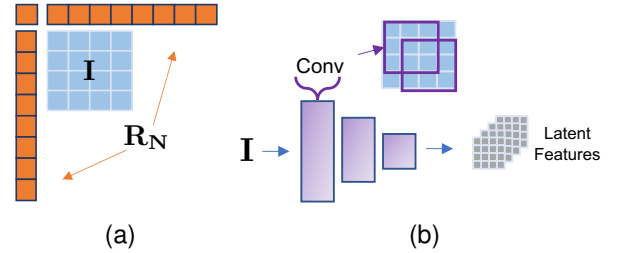


Fig. 3. **Nonlinear Transform.** (a) HiPT used in various Intra Profiles of H.264/AVC [57], HEVC [4], VVC [10], etc.; I is the block to be compressed; and R_N is a set of reconstructed neighbors. (b) Pretrained CNN transform with fixed weights used in [5]–[9].

valid neighbors from one stage to another but only needs to use small-kernel convolutions.

3 METHOD

Figure 2 depicts the network architecture used in our method. We follow the end-to-end VAE architecture [6] to construct main and hyper encoder-decoder pairs to layerwisely analyze and aggregate neighborhood information for R-D optimized compact representation. This work specifically focuses on the design of effective and efficient ANIA schemes in transform and entropy coding modules.

3.1 Content-Adaptive Transform via Stacked ICSAs

We realize the transform function by stacking ICSA units as shown in Fig. 2, where each ICSA unit is comprised of a convolutional layer and multiple RSTBs.

3.1.1 Theoretical Motivation

The leading performance of the HiPT used in VVC Intra suggests the effectiveness of the use of reconstructed neighbors to adaptively capture dynamic characteristics of the content.

As for a block **I** in Fig. 3a, the optimization process can be simply formulated from (1) as

$$\min_{m \in \Theta_m} E(\hat{c}_m) + E(m) + \lambda \cdot \text{MSE}(\mathbf{I}, \mathbf{I}_m^p + \hat{\mathbf{r}}_m), \quad (2)$$

$$\mathbf{I}_m^p = \mathbf{W}_m \mathbf{R}_N, \quad (3)$$

$$\hat{c}_m = Q(\text{DCT}(\mathbf{I} - \mathbf{I}_m^p)), \quad (4)$$

$$\hat{\mathbf{r}}_m = \text{IDCT}(\hat{c}_m), \quad (5)$$

where $\text{DCT}()$ and $\text{IDCT}()$ are DCT and inverse DCT applied on predictive residues. m is a predefined prediction mode from a set of candidate modes Θ_m specified in standards like VVC Intra [12]. For each mode m , standards also define particular means \mathbf{W}_m to weight reconstructed neighbors \mathbf{R}_N to form prediction \mathbf{I}_m^p [12]. Referring to (4), the DCT is often used with quantization $Q(\cdot)$ to generate quantized transform coefficients \hat{c}_m of predictive residues $\mathbf{r}_m = (\mathbf{I} - \mathbf{I}_m^p)$, yielding noise augmented residues $\hat{\mathbf{r}}_m$ in decoder for reconstruction. Here we use $E(\cdot)$ as the generic entropy coding engine for the coding of coefficients \hat{c}_m and side information m . In VVC [40], [58], notable CABAC is often used. Note that HiPT enforces the use of casual neighbors from available upper and/or left blocks of current **I** in Fig. 3a.

Such content-adaptive weighting of reconstructed neighbors in (3) allows us to leverage neighborhood dynamics to best exploit the redundancy of underlying non-stationary content, which however can not be supported by pretrained CNN transforms sketched in Fig. 3b because convolutional weights are fixed after training for subsequent task inference. It is naturally for us to explore whether we can also dynamically weigh and aggregate highly-correlated neighbors on-the-fly. Recalling that rate-distortion optimization of the VAE in Fig. 2 can be extended from (1) as

$$\min \mathbb{E}_{\mathbf{x} \sim p_{\mathbf{x}}} [-\log_2 p_{\hat{\mathbf{y}}}(\hat{\mathbf{y}}|\hat{\mathbf{z}})] + \mathbb{E}_{\mathbf{x} \sim p_{\mathbf{x}}} [-\log_2 p_{\hat{\mathbf{z}}}(\hat{\mathbf{z}})] + \lambda \cdot \mathbb{E}_{\mathbf{x} \sim p_{\mathbf{x}}} [d(\mathbf{x}, \hat{\mathbf{x}})], \quad (6)$$

$$\hat{\mathbf{y}} = Q(g_a(\mathbf{x})), \quad \hat{\mathbf{x}} = g_s(\hat{\mathbf{y}}), \quad (7)$$

$$\hat{\mathbf{z}} = Q(h_a(\mathbf{y})), \quad \text{params} = h_s(\hat{\mathbf{z}}), \quad (8)$$

where $p_{\mathbf{x}}$ is the distribution of input source image, $p_{\hat{\mathbf{y}}}$ and $p_{\hat{\mathbf{z}}}$ are the probability distribution of respective $\hat{\mathbf{y}}$ and $\hat{\mathbf{z}}$ at bottleneck layer used for entropy coding. Then the core issue is to find content-adaptive transformation matrices $g_a(\cdot)$, $g_s(\cdot)$, $h_a(\cdot)$ and $h_s(\cdot)$.

Luckily, recent surge of self-attention mechanism used in numerous Transformers [43] apparently offers the capacity to dynamically characterize and embed neighborhood information through attention-based weighting conditioned on the input. Thus, we propose to integrate the convolution layer and self-attention layer to fulfill the purpose as shown in Fig. 4a. Given that images and associated feature maps are basically a stack of 2D patches, it is straightforwardly for us to exemplify our idea using the Swin Transformer [25] that applies the Window-based Self-Attention mechanism.

3.1.2 Convolutional Token Embedding & Resampling

To ensure the spatial coherency as suggested in Vision Transformer studies [44], [45], we perform the convolutional token embedding shown in Fig. 4a to tokenize the input image $\mathbf{x} \in \mathbb{R}^{H \times W \times 3}$ for the first ICSA unit in Fig. 2 into

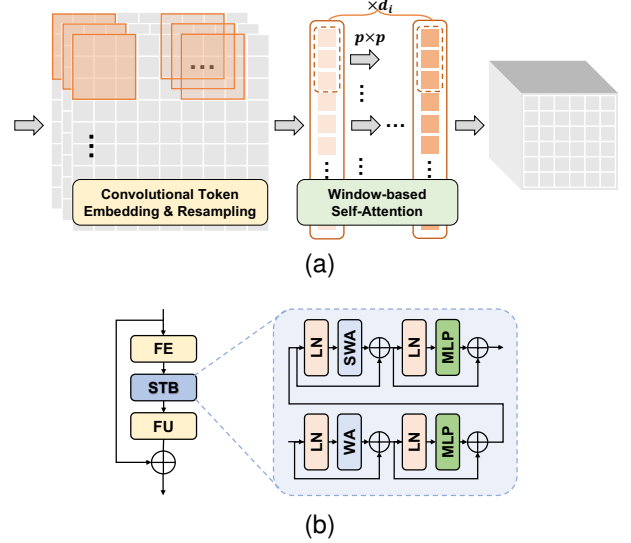


Fig. 4. **ICSA Unit**. (a) A convolutional layer is used for token embedding and spatial resampling followed by multiple (d_i) Window-based Self-Attention layers to aggregate attention-weighted neighbors on-the-fly. $p \times p$ is the size of attentive window. (b) Residual Swin Transformer Block (RSTB) [25] is used to enable Window-based Self-Attention. Please refer to [25] for more details regarding the Swin Transformer.

a latent space. The same tokenizations are enforced for subsequent ICSA units to process the output tensor from the RSTB module of proceeding ICSA for hierarchical token embedding. It is worth to point out that we also apply the spatial resampling at the convolution layer in each ICSA. This is because convolutions can aggregate and embed spatial neighbors within the receptive field to some extent, by which we can down-sample the resolution to reduce data dimensionality with negligible information loss. For simplicity, we apply the uniform sampling at each dimension with a stride of 2.

Since convolutional token embedding can implicitly encode the position information [59] to capture the spatial relationship between tokenized latents, it does not require the explicit position signaling in tokenization phase as reported in [44], [45]. Additionally, compared with non-overlapping pixel patches used in [48], convolutional token used for succeeding window-based self-attention computation can avoid blocky artifacts, and is beneficial to early visual processing and stable training as reported in [60], [61] and our simulations in Sec. 5.1.

3.1.3 Window-based Self-Attention via RSTB

Years ago, despite of the great success of Transformers in high-level vision tasks (e.g., classification) [44], [45], it is difficult to directly migrate the self-attention layer in Transformers to low-level vision tasks (e.g., compression) because of the quadruple computation complexity of input image size. Recently, the Swin Transformer [25] utilizes window-based self-attention, demonstrating outstanding efficiency with much less computation consumption.

As a result, we propose to stack multiple Residual Swin Transformer Blocks (RSTBs) right after the convolutional layer to form the ICSA unit. Figure 4b briefly sketches the structure of a RSTB where the first feature embedding (FE) layer projects input features at a size of $H \times W \times C$

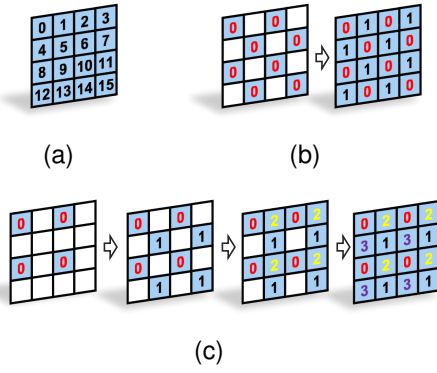


Fig. 5. **Spatial Patterning for Context Modeling.** (a) Sequential processing in a raster scan order used in AR model [6], [9]; (b) Two-stage parallel processing used in [30] and [64], [65] through the use of checkerboard pattern; (c) Multistage parallel processing. Non-overlapping 2×2 element blocks are used for spatial tiling, with elements labeled from 0 to 3 to represent consecutive processing stages from 0 to 3. Parallelism is enabled for elements marked with the same number; and context prediction is applied by masked convolution on valid local neighbors labeled with smaller number.

to a dimension of $HW \times C$, the following Swin Transformer Block (STB) which consists of the layer normalization (LN), window attention (WA), shifted window attention (SWA) and the MultiLayer Perceptron (MLP) layer aggregates neighborhood information through window-based self-attention, and finally a feature unembedding (FU) layer remaps attention-weighted features back to the original size of $H \times W \times C$. Residual connection is used for better information aggregation and model training [62]. The MLP layer is consist of two fully-connected layers and an activation layer GELU [63] is embedded in between.

Stacking RSTB not only enlarges the receptive field for information aggregation through the use of shifted window mechanism [25], but also offers the content-adaptive weighting and embedding of neighboring windows by self-attention computation.

3.2 Entropy Coding via Multistage Context Model

The use of joint hyperpriors and autoregressive neighbors for context modeling proposed in [6] brings significant R-D performance gain. However, the sharp increase of decoding complexity incurred by the processing of autoregressive neighbors is unacceptable, i.e., each latent feature token or element is calculated serially shown in Fig. 5a using causal neighbors through a masked convolution [20].

As strong correlation exists among local neighbors, instead of the sequential raster scan used in AR model, we propose an alternative spatial patterning shown in Fig. 5c to enable multistage context modeling where stage-wise parallel processing and neighborhood context prediction are easily fulfilled. A similar Two-stage Checkerboard Context Model was suggested by He *et al.* in [30], further confirming the advantages of the use of alternative scan order in context modeling of entropy coding for the pursuit of compression performance and computation throughput jointly. Compared with the checkerboard patterning exemplified in Fig. 5b, our MCM method offers better compression

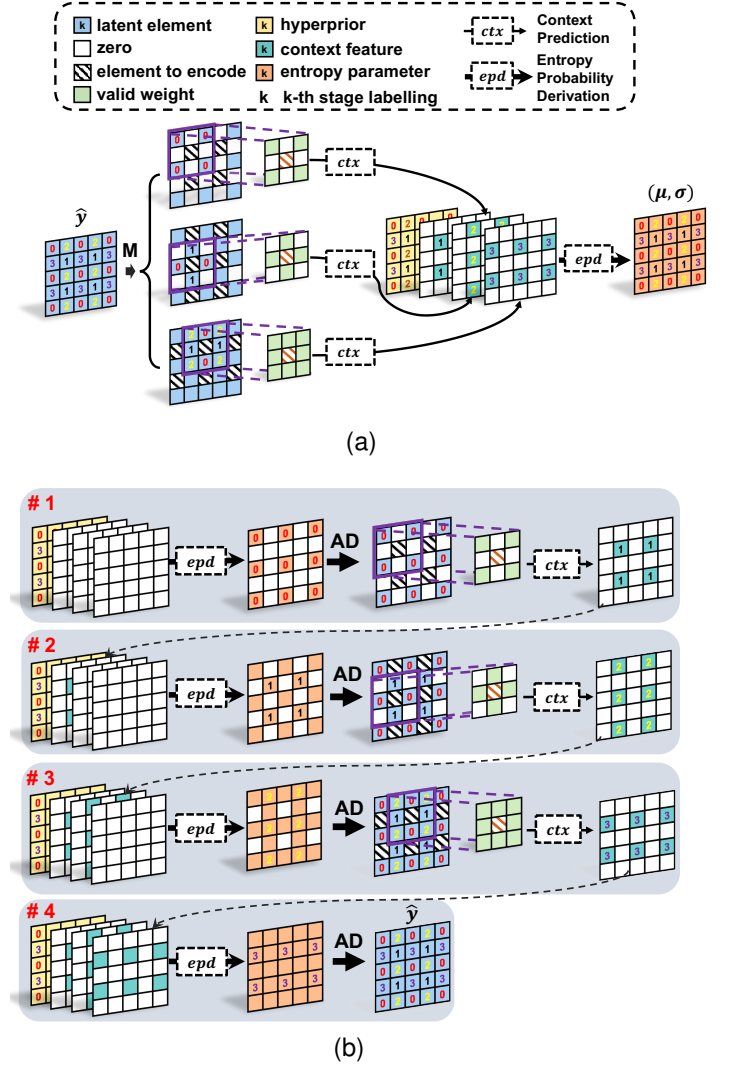


Fig. 6. **The Use of MCM.** (a) Parallel encoding (b) Multistage decoding. **M** represents binary masks, **AD** denotes the Arithmetic Decoding to derive latent elements. At decoder, massive parallelism can be achieved by processing latents at the same stage concurrently. Note that we perform spatial context modeling for all channels at one time, thus the channel dimension is omitted using 2D illustration for simplicity.

performance with the use of fine-grained local neighbors (see Table 3 and Fig. 13).

Next we offer detailed sketch on how to implement the Multistage Context Model (MCM) in entropy coding. As known, stacked convolutions used for entropy parameter determination and context prediction are the same for encoding and decoding as specified in Sec. 5.2.

3.2.1 One-stage Parallel Encoding

To efficiently encode latents \hat{y} , the probability of each element in \hat{y} shall be accurately estimated. Following the Gaussian distribution used in [6], [20], the probability estimation is reformulated as the derivation of entropy parameters (μ, σ) for all latents. Apparently, latent elements or tokens in \hat{y} are all available for encoding. This section shows how to derive entropy parameters concurrently following the use of MCM as plotted in Fig. 6a.

Recalling the spatial tiling using 2×2 element block in Fig. 5c and Fig. 6a, entropy parameters for upper-left latent

elements marked with “0” (e.g., stage#0 latents) are generated using corresponding stage#0 hyperpriors only through stacked 1×1 convolutions. Simultaneously, the entropy parameters of bottom-right stage#1 latents are generated using the stage#0 hyperpriors and stage#1 context features that are produced by 3×3 masked convolutions using four neighboring stage#0 latents. Similarly, the entropy parameters of stage#2 and stage#3 latents are generated using the same stage hyperpriors and context features that are derived using available and valid neighbors in a local 3×3 window, respectively.

Note that the determination of entropy parameters, a.k.a., *epd* module, at different stages shares the same stacked 1×1 convolutions to process concatenated hyperpriors and context features, and the context feature generation, i.e., *ctx* module, applies 3×3 masked convolutions to aggregate valid neighbors with stage-specific mask accordingly. Detailed settings for entropy parameters and context prediction are given at our project page. As will be unfolded in Sec. 5.2, we report that 3×3 convolution is sufficient for cross-stage context prediction which is due to the fact that the proposed content-adaptive transform offers more compact representation of input images with better redundancy removal. In practice, deploying 3×3 convolutions is more lightweight than existing works using 5×5 masked convolution [6], [20], [30].

3.2.2 Multistage Parallel Decoding

As depicted in Fig. 6b, four consecutive stages are involved in decoder to progressively reconstruct the latents \hat{y} , which basically mirrors the encoding operations. However, because of the casual dependency in decoding, it can only offer the parallel processing at the same stage.

- 1) At the first stage, only hyperpriors are used to generate the entropy parameters of stage#0 latents for entropy decoding and reconstruction; and then decoded stage#0 latents are processed with masked 3×3 convolutions to produce stage#1 context features for the second stage;
- 2) At the second stage, hyperpriors and stage#1 context features are processed to generate proper entropy parameters to reconstruct stage#1 latents that are subsequently convoluted to derive stage#2 context features;
- 3) At the third stage, both hyperpriors at stage#0 and context features at stage#1 and #2 are used to derive the entropy parameters to properly decode stage#2 latents; similarly stage#2 latents are then convoluted to derive stage#3 context features for the fourth stage;
- 4) In the end (at the fourth stage), we follow the same way in previous steps to reconstruct stage#3 latents to complete the \hat{y} .

Noted that the first and second step in proposed multistage decoding is almost the same as the two-stage decoding when applying the two-stage checkerboard context modeling in [30]. We call it “2CC” for comparison. Although the proposed MCM requires two more steps in decoding as compared with the 2CC model, it better exploits the neighborhood correlations with better performance.

4 EXPERIMENTAL EVALUATIONS

This section conducts comparative studies to understand the compression performance and complexity of the proposed *TinyLIC*.

4.1 Experimental Setup

Training. We choose the Flickr2W [66] as the training dataset in which image samples are randomly cropped into fixed patches at a size of $256 \times 256 \times 3$. More than 20k random patches are generated where 99% of them, i.e., 20k in total, are used for training, and the rest few hundreds patches are retained for quick model validation. Adam is used as the optimizer with default parameters provided in [67] and the batch size is set to 8 for each iteration. All training threads run on a single Titan RTX GPU for 400 epochs in total, having the learning rate at 10^{-4} initially, and then at 10^{-5} after 300 epochs.

Model Settings. Our *TinyLIC*, shown in Fig. 2, is implemented on top of the open-source CompressAI PyTorch library [68], by which we can easily share our models and materials for reproducible research. Eight models are trained from scratch to match 8 different bitrates (or quality levels) by adapting λ in (1). We set the number of feature channel to 128 for the first 4 models corresponding to low bit rates scenarios, and apply 192 channels for the rest 4 models to cover high bit rates. As for MSE loss used for distortion measurement, λ is chosen from $\{0.0018, 0.0035, 0.0067, 0.013, 0.025, 0.0483, 0.0932, 0.18\}$; while for MS-SSIM loss λ is from $\{2.40, 4.58, 8.73, 16.64, 31.73, 60.50, 115.37, 220.00\}$ ⁴. We later show at the supplemental website, very few models can cover the whole bitrate range without noticeable performance degradation.

For convolutional token embedding, we use small-scale 3×3 or 5×5 convolutional kernels for lightweight computation, and simply enforce the resampling by a stride of 2 at each spatial dimension. The number of RSTBs for four ICSA units in main coder are 2, 4, 6, and 2 respectively, i.e., $d_1 = 2, d_2 = 4, d_3 = 6$; And they are 2 and 2 in hyper coder, i.e., $d_5 = 2$ and $d_6 = 2$. The numbers of heads used in self-attention layer for RSTBs at four stages of main coder are 8, 8, 8 and 16; while they are fixed at 16 in hyper. The window size is 8×8 for RSTBs in main coder, while it is 4×4 in hyper coder; And the hidden channels are expanded by a factor of 2 for all MLP layers used in our work.

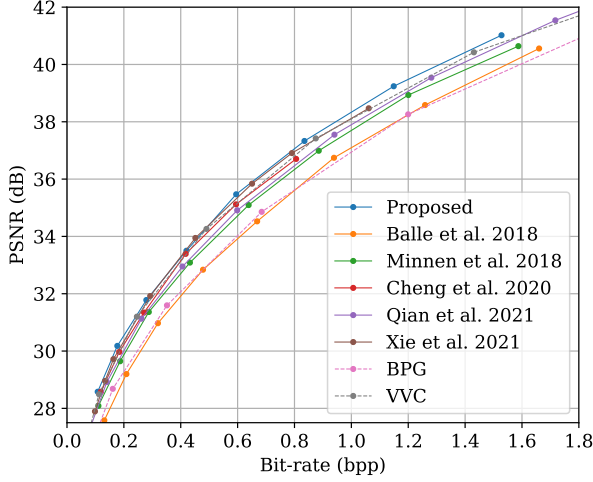
Testing. We use three popular datasets that contain diverse images for evaluation, i.e., the Kodak dataset⁵ with image sample at a size of 768×512 , Tecnick dataset⁶ with the image size of 1200×1200 and CLIC professional validation dataset⁷ which contains 41 images with 2k spatial resolution approximately. These datasets are widely used for image coding competitions. Both peak signal-to-noise ratio (PSNR) and MS-SSIM are used to quantify the decoded image quality; and the bits per pixel (bpp) measures the compressed bitrate.

4. In implementation the actual loss functions are $\lambda \times 255^2 \times D + R$ for MSE oriented optimization and $\lambda \times (1 - D) + R$ for the optimization using MS-SSIM as suggested in [68].

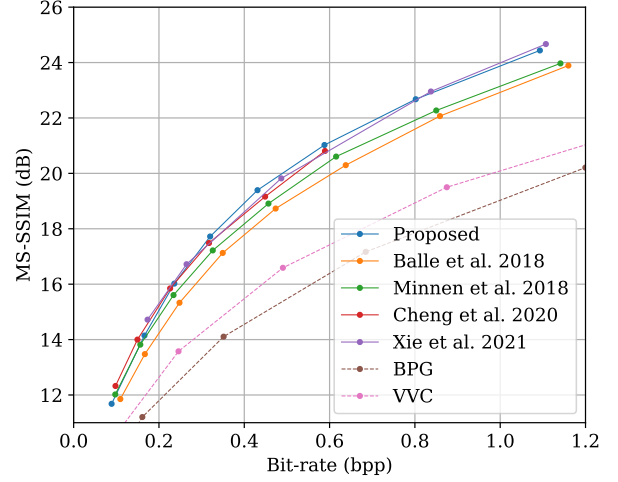
5. <https://r0k.us/graphics/kodak/>

6. https://tecnick.com/?aiocp_dp=testimages

7. <http://compression.cc/tasks/#image>



(a)



(b)

Fig. 7. R-D performance averaged on Kodak dataset: (a) MSE loss; (b) MS-SSIM loss.

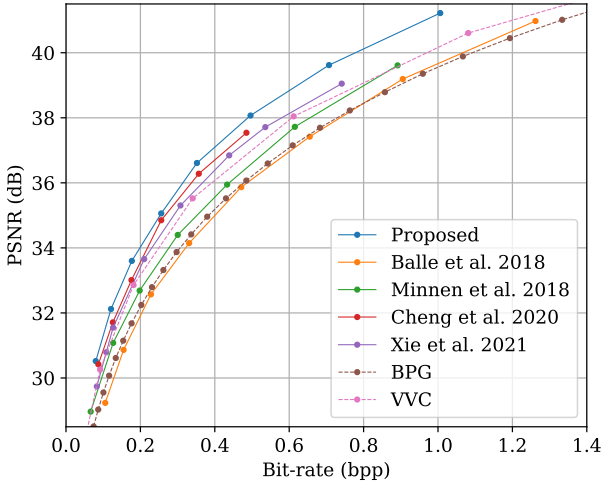


Fig. 8. R-D performance averaged on Tecnick dataset.

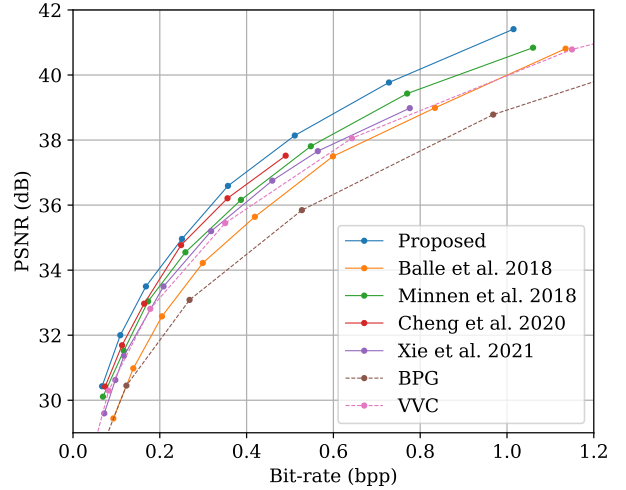


Fig. 9. R-D performance averaged on CLIC dataset.

4.2 Evaluation

Anchor & Alternatives. We set HEVC Intra compliant BPG method as the anchor, a.k.a., BPG, to derive BD-rate gains. We also offer the results of VVC Intra using its reference software VTM-12.1, a.k.a., VVC, to demonstrate the state-of-the-art image coding performance [12]. Meanwhile a broad collection of prominent learned LIC solutions are included for comparison with their best-produced results, including the Ballé *et al.* 2018 [5], Minnen *et al.* 2018 [6], Cheng *et al.* 2020 [9], Qian *et al.* 2021 [8], and Xie *et al.* 2021 [7]. These methods are representative examples plotting the technical development and coding efficiency progress for past years as discussed in Sec. 2.

4.2.1 Quantitative Performance

Rate-distortion (R-D) curves are plotted in Fig. 7, 8, 9 while the BD-rate gains against the BPG anchor are given in Table 2 and Fig. 1. For fair comparison, we try our best to ensure similar bitrate range across different approaches [28].

Overall BD-rate Gain. As for the results tested on Kodak dataset, the proposed method outperforms all other solutions for the distortion measured by both PSNR and MS-SSIM shown in Fig. 7. In Table 2, our method provides 22.23% BD-rate improvement against the anchor BPG, while the VVC just offers 18.07% gain. Coding gains are further enlarged for Tecnick and CLIC datasets as illustrated in Fig. 8 and 9. For instance, $\approx 15\%$ relative gain is captured for CLIC images that are widely used for image compression competitions, e.g., 41.54% BD-rate improvement to BPG for

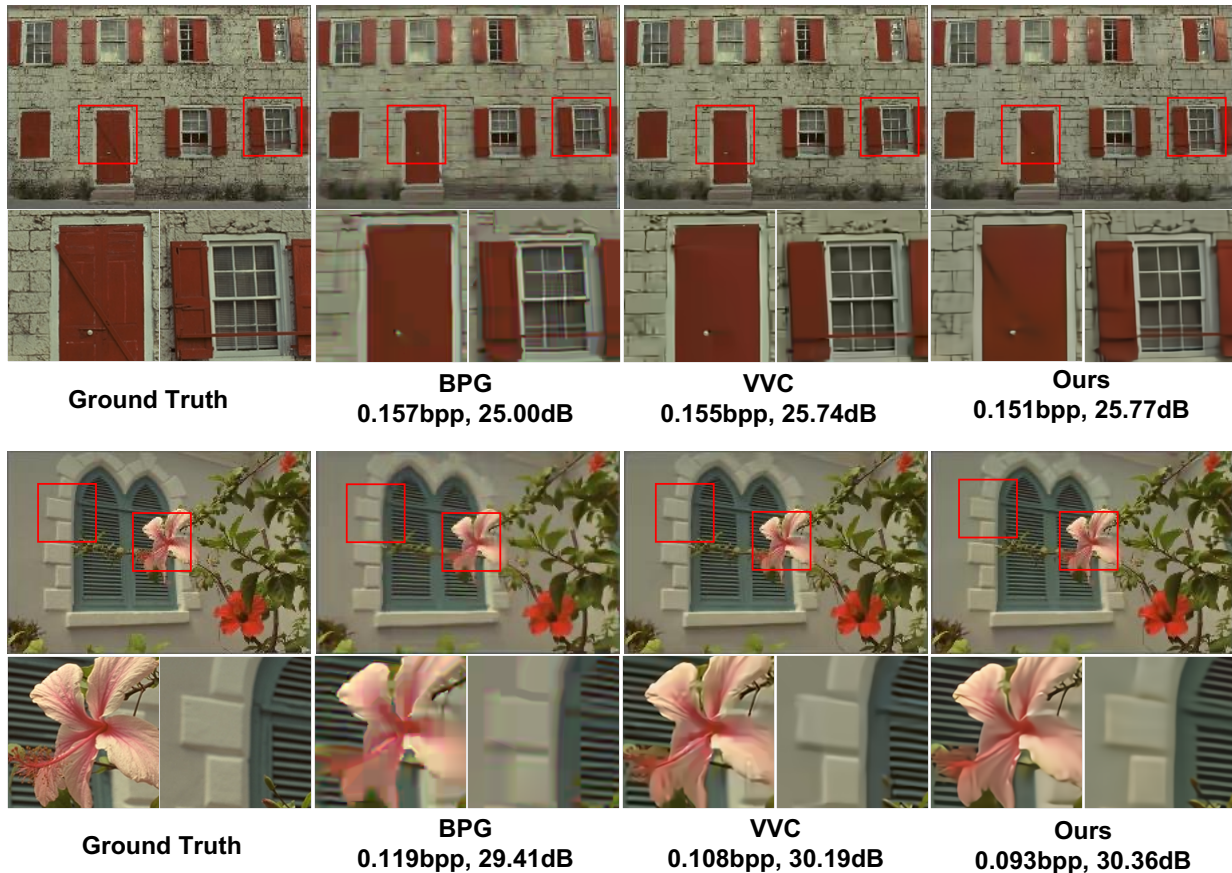


Fig. 10. **Qualitative Visualization.** Reconstructions and close-ups of the BPG, VVC and our method. Corresponding bpp and PSNR are marked.

TABLE 2
Averaged BD-rate improvement against the BPG anchor for different datasets. **Red** and **blue** indicates the best and the second best performance, respectively.

Method	Dataset Resolution	BD-rate (%) ↓
Ballé <i>et al.</i> 2018 [41]	Kodak 768 × 512	3.70
Minnen <i>et al.</i> 2018 [6]		-11.53
Cheng <i>et al.</i> 2020 [9]		-18.83
Xie <i>et al.</i> 2021 [7]		-21.60
VVC		-18.07
Ours - TinyLIC		-22.23
Ballé <i>et al.</i> 2018 [41]	Tecnick 1200 × 1200	3.08
Minnen <i>et al.</i> 2018 [6]		-11.91
Cheng <i>et al.</i> 2020 [9]		-29.35
Xie <i>et al.</i> 2021 [7]		-23.86
VVC		-19.28
Ours - TinyLIC		-34.42
Ballé <i>et al.</i> 2018 [41]	CLIC 2k	-14.10
Minnen <i>et al.</i> 2018 [6]		-32.13
Cheng <i>et al.</i> 2020 [9]		-37.92
Xie <i>et al.</i> 2021 [7]		-28.13
VVC		-25.60
Ours - TinyLIC		-41.53

“Ours” versus 25.63% of it for “VVC” in Table 2. In the mean time, our method also shows consistent performance lead in

comparison to other notable learned LICs.

Discussion. Almost all solutions report the increase of coding efficiency for test images with larger resolution in Table 2. For instance, averaged BD-rate gain for CLIC dataset is larger than it for Kodak dataset. This is because: image sample with larger spatial resolution would exhibit higher local coherency, for which it is easier to exploit neighborhood correlation for better compression efficiency.

It evidences that the VAE architecture with entropy context conditioned on joint hyperprior and local neighbors used in [6], [9], [20], [26] is a well generalized solution regardless of the different techniques used in its modular components like ReLU or GDN based activation, simple convolution or ICSA, etc. A slight performance inconsistency is spotted for Xie *et al.* 2021 [7] among testing datasets, e.g., ranked as the second best for Kodak dataset, but only fourth place for CLIC. This is largely because a different structure using invertible neural network and feature enhancement network is applied in Xie *et al.* 2021 [7].

Attention mechanism further reveals its outstanding effectiveness to adaptively weight and aggregate highly correlated information from the results of Cheng *et al.* 2020 [9] and our TinyLIC. Compared with Cheng *et al.* 2020 [9], our method not only extends the attention embedding to all stages (but not just the bottleneck layer) in main and hyper coders, but also replace the convolution-based attention computation with the self-attention to flexibly characterize the correlation of underlying dynamic content.

TABLE 3
Averaged encoding / decoding latency for Kodak dataset. 2CC is 2-stage Checkerboard Context modeling. Latency is measured by ms (millisecond) collected on Python platform.

Method	BD-rate (%) ↓	Latency (ms) ↓	
		Encoder	Decoder
Minnen <i>et al.</i> 2018 [6]	-11.53	56	1239
Cheng <i>et al.</i> 2020 [9]	-18.83	139	1332
Ours w/ CW	-21.35	262	231
Ours w/ 2CC	-20.78	147	107
Ours	-22.23	155	113

The VVC Intra is expected to succeed its predecessor HEVC Intra because of its outstanding performance [12]. We then switch the anchor from BPG to VVC to derive coding gains of the proposed *TinyLIC*, and $\approx 15\%$ BD-rate gains are captured on average across all three datasets.

4.2.2 Qualitative Visualization

Fig. 10 visualizes the reconstructions and closeups generated by the BPG, VVC, and our method. Ground-truth labels are also provided for side-by-side illustration. We particularly use the VVC compressed image for qualitative comparison because a set of normative in-loop filters are enabled in VVC intra coding which promises outstanding subjective quality of decoded image [69]. As seen, the proposed method noticeably improves the subjective quality with more sharp textures and less noise. Reconstruction snapshots of other test images from different datasets will be shown at the webpage.

4.2.3 Complexity

Three metrics are used for complexity measures, including the MACs/pixel, model size, and decoding latency in milliseconds.

Model Sizes and MACs. We first report the MACs/pixel and model size of each learned LIC solution in Fig. 1. As seen clearly, the proposed method provides the most competitive tradeoff between the compression gain and complexity consumption. Compared with the Minnen *et al.* 2018 [6] - a foundation work for other learned LICs, the proposed *TinyLIC* uses a much smaller model, e.g., $\approx 40\%$ model size reduction from 14.13M to 8.85M, less MACs/pixel with 8% reduction, e.g., from 412.72 to 378.65, but provides more than 10% relative BD-rate improvement to the same BPG anchor. Although Xie *et al.* 2021 [7] offers the closest BD-rate gain (e.g., -21.6% versus -22.23% in Table 2), its model size is about $5\times$, and its MACs/pixel is also close to $4\times$ of *TinyLIC*.

Decoding Latency. Image decoding latency was a pain point previously because of the sequential processing used in AR model. As shown in Table 3, our *TinyLIC* using MCM in default for entropy coding offers almost $10\times$ decoding speedup in comparison to Minnen *et al.* 2018 [6] and Cheng *et al.* 2020 [9] that both rely on the AR model leveraging the hyperprior and autoregressive neighbors jointly in entropy engine.

Another two context model aiming for reducing decoding latency are also included for comparison. One is the channel-wise (CW) context model proposed in [49], dubbed

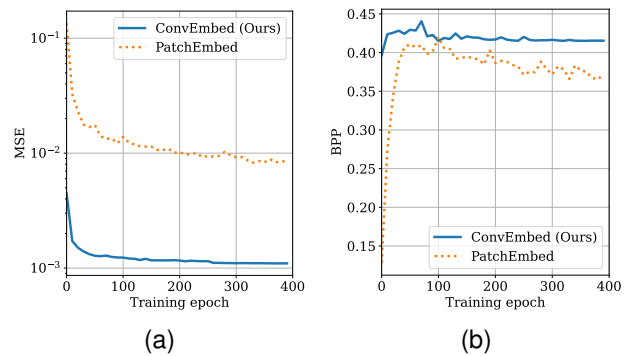


Fig. 11. **Token Embedding.** (a) $\log(\text{MSE})$ versus epoch (b) BPP versus epoch.

as the “Ours w/ CW” in Table 3; while the second one is two-stage checkerboard context (2CC) model, noted as “Ours w/ 2CC”. Such 2CC method is also applied in [30]. Here we mainly compare the computation throughput of CW and 2CC context models; while the details on compression performance are given in Sec. 5.2.

As seen, the proposed MCM clearly provides better performance and throughput trade-off. For example, compared with “Ours w/ CW”, almost 50% decoding latency reduction is observed (e.g., 231 ms vs. 113ms) with even better compression performance. Similarly, although two-stage checkerboard processing in “Ours w/ 2CC” can reduce the decoding latency to the similar level as the proposed MCM (e.g., 107 ms vs. 113 ms), but its compression performance is still inferior.

Note that the latency measurement is conducted on Python platform. Numbers may be different on other platforms but the trend would retain. Encoding latency is also provided for illustrative purpose since the throughput is not an critical issue at encoding phase.

5 ABLATION STUDIES

In this section, we dissect the *TinyLIC* to offer more insightful discussions on its modular components like the transform block backbone and entropy context models.

5.1 Transform Block Backbone

The *TinyLIC* stacks ICSA units to form the transform block backbone in default.

5.1.1 Token Embedding

Our ICSA applies a convolutional layer to do token embedding, noted as “ConvEmbed”. Apparently, there are many other solutions for the same purpose. One prevailing method can directly extract non-overlapping patches from input feature tensor for token embedding. We then follow the implementation in [48] to perform patch-based token embedding, a.k.a., “PatchEmbed”, to replace default “ConvEmbed” in *TinyLIC*. As shown in Fig. 11, we can clearly notice that default “ConvEmbed” provides much faster convergence rate than the “PatchEmbed” in model training. This coincides with the claim in [70], e.g., convolutional token

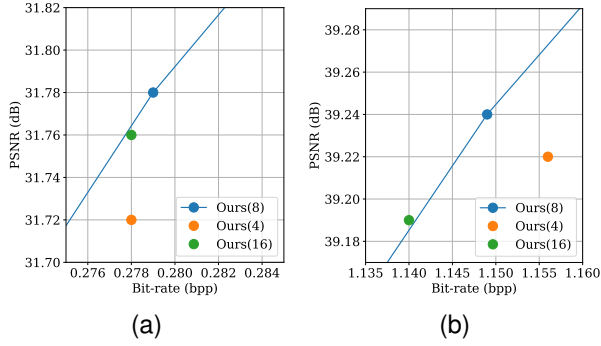


Fig. 12. **Attentive Window Size.** (a) Low bitrate with $\lambda = 0.0067$, (b) High bitrate with $\lambda = 0.0932$. Solid line is R-D curve of default *TinyLIC*.

embedding can improve the convergence stability of model. Other advantages of the use of “ConvEmbed” like implicit position embedding, flexible token size support, etc, can be referred in [70] as well.

5.1.2 Self-Attention Window Size

To understand the impact of window size in window-based self-attention layer of RSTB, we further examine 4×4 and 16×16 window settings in addition to the default 8×8 . Since the square window is used, we label them using “Ours(4)”, “Ours(8)” and “Ours(16)” respectively as in Fig. 12. Two different λ s at 0.0067 and 0.0932 are experimented for typical low and high bitrate scenarios.

When using 4×4 window, the performance drops slightly (≈ 0.04 dB) while the performance keeps unchanged for 16×16 attentive window, e.g., overlapped with default R-D curve. When compared with the default 8×8 window, proportionally more patches are used for 4×4 window, leading to the sharp increase of model parameters and potential throughput bottleneck; although less patches are used for 16×16 attentive window, per window computation is increased and it also imposes more strict resolution limitations of input content⁸. All of these suggest the 8×8 window is a justified option for balanced tradeoff.

5.1.3 Self-Attention vs. Large-kernel Convolution

Recently, large-kernel convolutions have promised comparable performance and complexity to window-based self-attention in Swin Transformer [25] as detailed in ConvNeXt [51]. This is because a large-kernel convolution enlarges the receptive field of neighborhood which is similar as the *shift* window mechanism in Swin Transformer. We then replace the self-attention block, e.g., RSTB, in *TinyLIC* with the ConvNeXt blocks (denoted as “w/ CNXB”) and retrain the model. As listed in the last row of Table 4, when using the same training dataset, the new model using large-kernel convolutions, a.k.a., “w/ CNXB”, is just slightly worse than the default *TinyLIC* that uses the RSTB in default (“w/ RSTB”), presenting 1.20% relative BD-rate loss. This definitely shows that a larger receptive field incurred by the large-kernel convolution could offer better compression

8. The input image size should be a multiple of $2^6 \times w^2$ since resampling by a stride of 2 at each dimension is enforced 6 times as pictured in Fig. 2. Here w is the side length of a square.

TABLE 4
Relative BD-rate loss When randomly-sampling the training dataset to different volume scales.

Method	volume scale (%)	BD-rate (%) \downarrow
w/ CNXB	10	33.25
w/ RSTB		25.31
w/ CNXB	25	14.92
w/ RSTB		9.92
w/ CNXB	75	1.95
w/ RSTB		0.05
w/ CNXB	default	1.20
w/ RSTB (default)		-

efficiency when compared with proceeding works mainly using small-kernel convolutions like 3×3 .

The results shown in the last row of Table 4 may lead to a claim: capturing relatively long-range dependency by either window-based self-attention or large-kernel convolution could potential improve the performance of underlying tasks. Besides, we believe that window-based self-attention can adaptively characterise dynamic content accordingly for better information weighting and aggregation which however is not easily supported by fixed-weights CNN models. To prove it, we randomly subsample the training dataset to respective 75%, 25% and 10% of its original volume scale, and faithfully retrain the default *TinyLIC* with self-attention (“w/ RSTB”) and modified *TinyLIC* with large-kernel convolution (“w/ CNXB”) accordingly. As reported in Table 4, the relative BD-rate loss of “w/ RSTB” is less than it of “w/CNXB”, which confirms our hypothesis. It is worth to point out that, when having 75% samples from the original training dataset, default *TinyLIC* can still provide convincing BD-rate with negligible loss, e.g., 0.05%.

In a summary, the proposed ICSA unit can jointly leverage the advantages of convolution and self-attention to form the effective content-adaptive transform to dynamically weigh and aggregate neighborhood information of given input for robust compression with better efficiency.

5.2 Entropy Context Model

This section comprehensively examines entropy context models for insightful comparison.

5.2.1 Alternative Model

First of all, the seminal context model using joint hyperprior and autoregressive neighbors (AR) [6] is the foundation of succeeding works. As aforementioned, data dependency in AR model limits the processing in a sequential manner, leading to unbearable decoding latency. Since then, a serial refinements have been developed and tried to alleviate the autoregressive dependency for better throughput, such as the channel-wise grouping (CW) [49], two-stage checkerboard patterning (2CC) [30] and the proposed MCM, etc.

We replace the default MCM in entropy coding with respective CW model [49] (“Ours w/ CW”), and the most notable AR model [6] (“Ours w/ AR”), and retrain them for comparison. As shown in Fig. 13, the AR model still leads the BD-rate improvement, but with marginal gain to the proposed MCM (“Ours”), e.g., with less 0.05 dB loss at

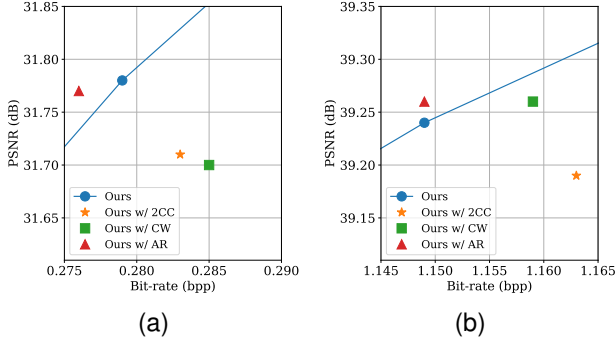


Fig. 13. Entropy Context Models. (a) Low bitrate with $\lambda = 0.0067$, (b) High bitrate with $\lambda = 0.0932$. Solid line is R-D curve of default *TinyLIC*.

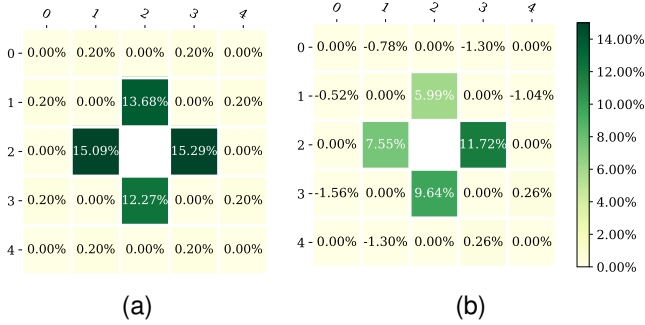


Fig. 14. Rate Saving Ratio Contributed by Neighbors in local 5×5 Window. (a) CNN backbone from Minnen *et al.* [6] for nonlinear transform, (b) Proposed content-adaptive transform backbone using stacked ICSAs (Ours). Simulations are tested on Kodak images. Masked convolution is set with 5×5 kernel as in [30].

the similar bitrate. However, our MCM could significantly speedup the decoding as reported in Table 3. The CW model exhibits inferior performance at both low and high bitrates, particularly at low bitrates (e.g., more than 0.15 dB loss captured).

5.2.2 Multistage Context Prediction

Masked convolutions are properly used for context prediction in proposed MCM to aggregate neighborhood information stagewise. As aforementioned, a two-stage checkerboard context model - 2CC (see Fig. 5b) can be also devised to speedup decoding without autoregressive dependency. The BD-rate performance of the 2CC model is also provided, a.k.a, “Ours w/ 2CC” in Fig. 13 which confirms the performance comparison in Table 3. Having more stages can help to gradually leverage more close neighborhood elements for context prediction.

As a matter of fact, each decoding step of the proposed MCM shown in Fig. 6b can be treated as a two-stage checkerboard reconstruction. We then follow the methodology in [30] to collect the rate saving contribution from neighbors, as depicted in Fig. 14. To best emulate the environment in [30], we experimentally enlarge the kernel size to 5×5 for masked convolution and also adopt the CNN backbone from Minnen *et al.* 2018 [6] for nonlinear

TABLE 5
Progressive Rate Reduction Contributed by Context Models Used in Multiple Stages. (Results Are Averaged on Kodak Set with $\lambda = 0.0067$; Similar Outcomes Are Observed for Other λ s).

hyperpriors	ctx#1	ctx#2	ctx#3	bpp ↓
✓				0.480
✓			✓	0.396
✓		✓	✓	0.313
✓	✓	✓	✓	0.279

transform. As seen, the closer the neighbors, the higher rate saving contributions, confirming the observations in [30].

Comparing the subplots in Fig. 14, e.g., Fig. 14a vs. Fig. 14b, we first notice that rate savings contributed by neighbors are larger for CNN transforms. This is because our proposed content-adaptive transform using integrated convolution and self-attention can better exploit the redundancy with more compact representation, leaving less room for correlation exploration in entropy coding. Another interesting observation is that the rate saving contribution is negative for neighbors outside the 3×3 window centered at current element in Fig. 14b, suggesting that a 3×3 kernel is sufficient for masked convolution in the proposed MCM.

In addition, we also report the rate reduction contributed by multistage contexts in Table 5. As seen, by only enabling the hyperpriors (by completely ignoring stage-wise contexts), the bpp value increases sharply with much higher value than the default setting using both hyperpriors and multistage context models in *TinyLIC*. By enabling the context prediction for latent elements (e.g., ctx# k represents the use of context model in stage# k , $k = 1, 2, 3$) from stage#1 to stage#3, more bit saving is reported, clearly evidencing the effectiveness of our proposed MCM to gradually aggregate neighborhood information.

6 CONCLUSION

A novel learned image coding method - *TinyLIC* was developed in this work, presenting the superior compression performance, e.g., averaged 15% BD-rate gains against the VVC Intra anchor, and high-throughput computation, e.g., almost $10\times$ decoding speedup compared with prominent learned lossy image coding approaches.

Joint high-performance compression and high throughput computation of the proposed *TinyLIC* comes from the intelligent use of adaptive neighborhood information aggregation. To this aim, we integrate the convolution and self-attention to form the content-adaptive transform by which we can dynamically characterize and embed the neighborhood information conditioned on the input content; we further propose the multistage context model using local neighbors for entropy coding to unknit the autoregressive dependency for parallel processing while still retaining the efficiency as the autoregressive model.

A companion webpage is also offered to demonstrate that the proposed *TinyLIC* can be easily extended with the support of variable-rate compression, different input source, etc, further revealing the generalization of the proposed method and promising prospect for practical applications.

ACKNOWLEDGEMENT

We particularly thank the authors of Ballé *et al.* 2018 [5], Minnen *et al.* 2018 [6], Cheng *et al.* 2020 [9], Qian *et al.* 2021 [8], Xie *et al.* 2021 [7] for their publicly accessible models and materials used in our comparative studies.

REFERENCES

- [1] J. D. Gibson, "Rate distortion functions and rate distortion function lower bounds for real-world sources," *Entropy*, vol. 19, p. 604, 2017. **1**
- [2] J. Ballé, P. A. Chou, D. Minnen, S. Singh, N. Johnston, E. Agustsson, S. J. Hwang, and G. Toderici, "Nonlinear transform coding," *IEEE Journal of Selected Topics in Signal Processing*, vol. 15, no. 2, pp. 339–353, 2020. **1, 2, 3**
- [3] V. Goyal, "Theoretical foundations of transform coding," *IEEE Signal Processing Magazine*, vol. 18, no. 5, pp. 9–21, 2001. **1, 3**
- [4] G. J. Sullivan, J.-R. Ohm, W.-J. Han, and T. Wiegand, "Overview of the high efficiency video coding (hevc) standard," *IEEE Transactions on Circuits and Systems for Video Technology*, vol. 22, no. 12, pp. 1649–1668, 2012. **1, 2, 3, 5**
- [5] J. Ballé, D. Minnen, S. Singh, S. J. Hwang, and N. Johnston, "Variational image compression with a scale hyperprior," in *International Conference on Learning Representations*, 2018. **1, 3, 5, 9, 14**
- [6] D. Minnen, J. Ballé, and G. Toderici, "Joint autoregressive and hierarchical priors for learned image compression," in *Advances in Neural Information Processing Systems*, 2018, pp. 10 794–10 803. **1, 2, 3, 4, 5, 7, 8, 9, 10, 11, 12, 13, 14**
- [7] Y. Xie, K. L. Cheng, and Q. Chen, "Enhanced invertible encoding for learned image compression," in *Proceedings of the ACM International Conference on Multimedia*, 2021. **1, 5, 9, 10, 11, 14**
- [8] Y. Qian, Z. Tan, X. Sun, M. Lin, D. Li, Z. Sun, L. Hao, and R. Jin, "Learning accurate entropy model with global reference for image compression," in *International Conference on Learning Representations*, 2020. **1, 4, 5, 9, 14**
- [9] Z. Cheng, H. Sun, M. Takeuchi, and J. Katto, "Learned image compression with discretized gaussian mixture likelihoods and attention modules," in *Proceedings of the IEEE/CVF Conference on Computer Vision and Pattern Recognition*, 2020, pp. 7939–7948. **1, 2, 3, 4, 5, 7, 9, 10, 11, 14**
- [10] B. Bross, Y.-K. Wang, Y. Ye, S. Liu, J. Chen, G. J. Sullivan, and J.-R. Ohm, "Overview of the versatile video coding (vvc) standard and its applications," *IEEE Transactions on Circuits and Systems for Video Technology*, vol. 31, no. 10, pp. 3736–3764, 2021. **1, 2, 3, 5**
- [11] J. Lainema, F. Bossen, W.-J. Han, J. Min, and K. Ugur, "Intra coding of the hevc standard," *IEEE Trans. Circuits Syst. Video Technol.*, vol. 22, no. 12, pp. 1792–1801, Dec. 2012. **1, 2, 4**
- [12] J. Pfaff, A. Filippov, S. Liu, X. Zhao, J. Chen, S. De-Luxán-Hernández, T. Wiegand, V. Ruffitskiy, A. K. Ramasubramanian, and G. Van der Auwera, "Intra prediction and mode coding in vvc," *IEEE Transactions on Circuits and Systems for Video Technology*, vol. 31, no. 10, pp. 3834–3847, 2021. **1, 2, 4, 6, 9, 11**
- [13] R. M. Gray and D. L. Neuhoff, "Quantization," *IEEE Transactions on Information Theory*, vol. 44, no. 6, pp. 2325–2383, Oct 1998. **1**
- [14] D. Marpe, H. Schwarz, and T. Wiegand, "Context-based adaptive binary arithmetic coding in the h.264/avc video compression standard," *IEEE Transactions on Circuits and Systems for Video Technology*, vol. 13, no. 7, pp. 620–636, 2003. **2, 4**
- [15] G. J. Sullivan and T. Wiegand, "Video compression—from concepts to the H.264/AVC standard," *Proceedings of the IEEE*, vol. 93, no. 1, pp. 18–31, 2005. **2**
- [16] Overview of JPEG, "<https://jpeg.org/jpeg/>," 2018. **2, 4**
- [17] D. T. Lee, "Jpeg 2000: Retrospective and new developments," *Proceedings of the IEEE*, vol. 93, no. 1, pp. 32–41, Jan 2005. **2**
- [18] N. Ahmed, T. Natarajan, and K. R. Rao, "Discrete cosine transform," *IEEE transactions on Computers*, vol. 100, no. 1, pp. 90–93, 1974. **2, 3**
- [19] X. Zhang, C. Yang, X. Li, S. Liu, H. Yang, I. Katsavounidis, S.-M. Lei, and C.-C. J. Kuo, "Image coding with data-driven transforms: Methodology, performance and potential," *IEEE Transactions on Image Processing*, vol. 29, pp. 9292–9304, 2020. **2, 3, 4**
- [20] T. Chen, H. Liu, Z. Ma, Q. Shen, X. Cao, and Y. Wang, "End-to-end learnt image compression via non-local attention optimization and improved context modeling," *IEEE Transactions on Image Processing*, vol. 30, pp. 3179–3191, 2021. **2, 3, 4, 5, 7, 8, 10**
- [21] P. Belememis, N. Panagou, T. Loukopoulos, and M. Koziri, "Review and comparative analysis of parallel video encoding techniques for VVC," in *Applications of Digital Image Processing XLIII*, A. G. Tescher and T. Ebrahimi, Eds., vol. 11510, International Society for Optics and Photonics. SPIE, 2020, pp. 258 – 276. [Online]. Available: <https://doi.org/10.1117/12.2569283> **2**
- [22] V. Sze and M. Budagavi, "High throughput cabac entropy coding in hevc," *IEEE Transactions on Circuits and Systems for Video Technology*, vol. 22, no. 12, pp. 1778–1791, 2012. **2, 4**
- [23] J. Liang, J. Cao, G. Sun, K. Zhang, L. Van Gool, and R. Timofte, "Swinir: Image restoration using swin transformer," in *IEEE International Conference on Computer Vision Workshops*, 2021. **2**
- [24] X. Jia, B. De Brabandere, T. Tuytelaars, and L. V. Gool, "Dynamic filter networks," *Advances in neural information processing systems*, vol. 29, 2016. **2**
- [25] Z. Liu, Y. Lin, Y. Cao, H. Hu, Y. Wei, Z. Zhang, S. Lin, and B. Guo, "Swin transformer: Hierarchical vision transformer using shifted windows," *International Conference on Computer Vision (ICCV)*, 2021. **2, 4, 6, 7, 12**
- [26] M. Lu, P. Guo, H. Shi, C. Cao, and Z. Ma, "Transformer-based image compression," in *IEEE Data Compression Conference*, 2022. **2, 4, 10**
- [27] H. Liu, M. Lu, Z. Chen, X. Cao, Z. Ma, and Y. Wang, "End-to-end neural video coding using a compound spatiotemporal representation," *IEEE Transactions on Circuits and Systems for Video Technology*, pp. 1–1, 2022. **2**
- [28] G. Bjontegaard, "Calculation of average PSNR differences between R-D curves," in *Doc. VCEG-M33, ITU-T VCEG 13th Meeting*, 2001. **2, 9**
- [29] Z. Wang, E. P. Simoncelli, and A. C. Bovik, "Multiscale structural similarity for image quality assessment," in *The Thirty-Seventh Asilomar Conference on Signals, Systems & Computers*, 2003, pp. 1398–1402. **2**
- [30] D. He, Y. Zheng, B. Sun, Y. Wang, and H. Qin, "Checkerboard context model for efficient learned image compression," in *Proceedings of the IEEE/CVF Conference on Computer Vision and Pattern Recognition*, 2021, pp. 14 771–14 780. **3, 5, 7, 8, 11, 12, 13**
- [31] B.-F. Wu and C.-F. Lin, "A high-performance and memory-efficient pipeline architecture for the 5/3 and 9/7 discrete wavelet transform of jpeg2000 codec," *IEEE Transactions on Circuits and Systems for Video Technology*, vol. 15, no. 12, pp. 1615–1628, 2005. **3**
- [32] G. K. Wallace, "The jpeg still picture compression standard," *IEEE transactions on consumer electronics*, vol. 38, no. 1, pp. xviii–xxxiv, 1992. **3**
- [33] M. Rabbani, "Jpeg2000: Image compression fundamentals, standards and practice," *Journal of Electronic Imaging*, vol. 11, no. 2, p. 286, 2002. **3**
- [34] A. T. Hinds, Y. A. Reznik, L. Yu, Z. Ni, and C. Zhang, "Drift analysis for integer IDCT," in *Applications of Digital Image Processing XXX*, A. G. Tescher, Ed., vol. 6696, International Society for Optics and Photonics. SPIE, 2007, pp. 432 – 447. [Online]. Available: <https://doi.org/10.1117/12.740220> **3**
- [35] H. Malvar, A. Hallapuro, M. Karczewicz, and L. Kerofsky, "Low complexity transform and quantization in H.264/AVC," *IEEE Trans. Circuits Syst. Video Technol.*, vol. 13, no. 7, pp. 598–603, Jul. 2003. **3**
- [36] Y. Xue and Y. Wang, "Video coding using a self-adaptive redundant dictionary consisting of spatial and temporal prediction candidates," in *Proc. IEEE Int. Conf. Multimedia and Expo (ICME)*, 2014. **3**
- [37] M. Xu, S. Li, J. Lu, and W. Zhu, "Compressibility constrained sparse representation with learnt dictionary for low bit-rate image compression," *IEEE Transactions on Circuits and Systems for Video Technology*, vol. 24, no. 10, pp. 1743–1757, 2014. **3**
- [38] K. Skretting and K. Engan, "Image compression using learned dictionaries by rls-dla and compared with k-svd," in *2011 IEEE International Conference on Acoustics, Speech and Signal Processing (ICASSP)*, 2011, pp. 1517–1520. **3**
- [39] X. Li and M. T. Orchard, "Edge-directed prediction for lossless compression of natural images," *IEEE Transactions on image processing*, vol. 10, no. 6, pp. 813–817, 2001. **4**
- [40] H. Schwarz, M. Coban, M. Karczewicz, T.-D. Chuang, F. Bossen, A. Alshin, J. Lainema, C. R. Helmrich, and T. Wiegand, "Quantization and entropy coding in the versatile video coding (vvc) standard," *IEEE Transactions on Circuits and Systems for Video Technology*, vol. 31, no. 10, pp. 3891–3906, 2021. **4, 6**

- [41] J. Ballé, V. Laparra, and E. P. Simoncelli, "End-to-end optimized image compression," in *International Conference on Learning Representations*, 2017. 4, 10
- [42] J.-H. Kim, B. Heo, and J.-S. Lee, "Joint global and local hierarchical priors for learned image compression," 2021. 4
- [43] K. Han, Y. Wang, H. Chen, X. Chen, J. Guo, Z. Liu, Y. Tang, A. Xiao, C. Xu, Y. Xu, Z. Yang, Y. Zhang, and D. Tao, "A survey on vision transformer," *IEEE Transactions on Pattern Analysis & Machine Intelligence*, no. 01, pp. 1–1, feb 5555. 4, 6
- [44] N. Carion, F. Massa, G. Synnaeve, N. Usunier, A. Kirillov, and S. Zagoruyko, "End-to-end object detection with transformers," in *European Conference on Computer Vision*. Springer, 2020, pp. 213–229. 4, 6
- [45] A. Dosovitskiy, L. Beyer, A. Kolesnikov, D. Weissenborn, X. Zhai, T. Unterthiner, M. Dehghani, M. Minderer, G. Heigold, S. Gelly et al., "An image is worth 16x16 words: Transformers for image recognition at scale," *arXiv preprint arXiv:2010.11929*, 2020. 4, 6
- [46] D. Zhou, B. Kang, X. Jin, L. Yang, X. Lian, Z. Jiang, Q. Hou, and J. Feng, "Deepvit: Towards deeper vision transformer," *arXiv:2103.11886*, 2021. 4
- [47] Z. Wang, X. Cun, J. Bao, and J. Liu, "Uformer: A general u-shaped transformer for image restoration," *arXiv:2106.03106*, 2021. 4
- [48] Y. Zhu, Y. Yang, and T. Cohen, "Transformer-based transform coding," in *International Conference on Learning Representations*, 2022. 4, 6, 11
- [49] D. Minnen and S. Singh, "Channel-wise autoregressive entropy models for learned image compression," in *2020 IEEE International Conference on Image Processing (ICIP)*. IEEE, 2020, pp. 3339–3343. 4, 5, 11, 12
- [50] Y. Qian, X. Sun, M. Lin, Z. Tan, and R. Jin, "Entroformer: A Transformer-based Entropy Model for Learned Image Compression," in *International Conference on Learning Representations*, 2022. 4
- [51] Z. Liu, H. Mao, C.-Y. Wu, C. Feichtenhofer, T. Darrell, and S. Xie, "A convnet for the 2020s," 2022. 4, 12
- [52] T. Chen and Z. Ma, "Variable bitrate image compression with quality scaling factors," in *ICASSP 2020-2020 IEEE International Conference on Acoustics, Speech and Signal Processing (ICASSP)*. IEEE, 2020, pp. 2163–2167. 5
- [53] Z. Sun, Z. Tan, X. Sun, F. Zhang, Y. Qian, D. Li, and H. Li, *Interpolation Variable Rate Image Compression*. New York, NY, USA: Association for Computing Machinery, 2021, p. 5574–5582. [Online]. Available: <https://doi.org/10.1145/3474085.3475698> 5
- [54] J. Lin, M. Akbari, H. Fu, Q. Zhang, S. Wang, J. Liang, D. Liu, F. Liang, G. Zhang, and C. Tu, "Variable-rate multi-frequency image compression using modulated generalized octave convolution," in *2020 IEEE 22nd International Workshop on Multimedia Signal Processing (MMSP)*, 2020, pp. 1–6. 5
- [63] D. Hendrycks and K. Gimpel, "Gaussian error linear units (gelus)," *arXiv preprint arXiv:1606.08415*, 2016. 7
- [55] J. Ballé, N. Johnston, and D. Minnen, "Integer networks for data compression with latent-variable models," in *International Conference on Learning Representations*, 2018. 5
- [56] W. Hong, T. Chen, M. Lu, S. Pu, and Z. Ma, "Efficient neural image decoding via fixed-point inference," *IEEE Transactions on Circuits and Systems for Video Technology*, vol. 31, no. 9, pp. 3618–3630, 2020. 5
- [57] T. Wiegand, G. J. Sullivan, G. Bjontegaard, and A. Luthra, "Overview of the H.264/AVC video coding standard," *IEEE Trans. Circuits Syst. Video Technol.*, vol. 13, no. 7, pp. 560–576, 2003. 5
- [58] X. Zhao, S.-H. Kim, Y. Zhao, H. E. Egilmez, M. Koo, S. Liu, J. Lainema, and M. Karczewicz, "Transform coding in the vvc standard," *IEEE Transactions on Circuits and Systems for Video Technology*, vol. 31, no. 10, pp. 3878–3890, 2021. 6
- [59] M. A. Islam, S. Jia, and N. D. Bruce, "How much position information do convolutional neural networks encode?" in *International Conference on Learning Representations*, 2019. 6
- [60] A. Gulati, J. Qin, C.-C. Chiu, N. Parmar, Y. Zhang, J. Yu, W. Han, S. Wang, Z. Zhang, Y. Wu et al., "Conformer: Convolution-augmented transformer for speech recognition," *arXiv preprint arXiv:2005.08100*, 2020. 6
- [61] T. Xiao, M. Singh, E. Mintun, T. Darrell, P. Dollár, and R. Girshick, "Early convolutions help transformers see better," *arXiv preprint arXiv:2106.14881*, 2021. 6
- [62] K. He, X. Zhang, S. Ren, and J. Sun, "Deep residual learning for image recognition," in *Proceedings of the IEEE Conference on Computer Vision and Pattern Recognition (CVPR)*, June 2016. 7
- [64] Z. Ma and A. Segall, "System for graceful power degradation," *Joint Collaborative Team on Video Coding (JCT-VC) of ITU-T SG16 WP3 and ISO/IEC JTC1/SC29/WG11, JCTVC-B114*, pp. 1–8, 2010. 7
- [65] —, "Frame buffer compression for low-power video coding," in *2011 18th IEEE International Conference on Image Processing*. IEEE, 2011, pp. 757–760. 7
- [66] J. Liu, G. Lu, Z. Hu, and D. Xu, "A unified end-to-end framework for efficient deep image compression," *arXiv preprint arXiv:2002.03370*, 2020. 8
- [67] D. P. Kingma and J. Ba, "Adam: A method for stochastic optimization," *arXiv preprint arXiv:1412.6980*, 2014. 8
- [68] J. Bégaïnt, F. Racapé, S. Feltman, and A. Pushparaja, "Compressai: a pytorch library and evaluation platform for end-to-end compression research," *arXiv preprint arXiv:2011.03029*, 2020. 8
- [69] M. Karczewicz, N. Hu, J. Taquet, C.-Y. Chen, K. Misra, K. Andersson, P. Yin, T. Lu, E. François, and J. Chen, "Vvc in-loop filters," *IEEE Transactions on Circuits and Systems for Video Technology*, vol. 31, no. 10, pp. 3907–3925, 2021. 11
- [70] H. Wu, B. Xiao, N. Codella, M. Liu, X. Dai, L. Yuan, and L. Zhang, "Cvt: Introducing convolutions to vision transformers," in *2021 IEEE/CVF International Conference on Computer Vision (ICCV)*, 2021, pp. 22–31. 11, 12